Composites Science and Technology 69 (2009) 2054–2063

Contents lists available at ScienceDirect

Composites Science and Technology

journal homepage: www.elsevier.com/locate/compscitech

Probability of the presence of damage estimated from an active sensor network in a composite panel of multiple stiffeners

Dong Wang [a], Lin Ye [a,b,*], Ye Lu [a], Zhongqing Su [b]

[a] Laboratory of Smart Materials and Structures (LSMS), Centre for Advanced Materials Technology (CAMT), School of Aerospace, Mechanical and Mechatronic Engineering, The University of Sydney, NSW 2006, Australia
[b] Department of Mechanical Engineering, The Hong Kong Polytechnic University, Hong Kong SAR, PR China

ARTICLE INFO

Article history:
Received 25 June 2008
Received in revised form 17 October 2008
Accepted 1 November 2008
Available online 14 November 2008

Keywords:
A. Smart materials
C. Probabilistic methods
D. Ultrasonics
D. Non-destructive testing

ABSTRACT

Artificial damage in the form of a through-thickness hole in a composite panel of five stiffeners is identified using a guided wave-based damage diagnostic algorithm, which is based on the probability of the presence of damage in the monitoring area estimated using correlation coefficients of Lamb wave signals from an active sensor network. Without defining the detail features of individual wave components, this diagnostic algorithm focuses on the calibrated changes in wave signals due to the presence of damage. The probability of the presence of damage at each grid in the monitoring area is estimated. The area consisting of grids with probability values for the presence of damage above a threshold is subsequently identified for damage identification. The effect of networks of sensing paths and shapes of the affected zone of individual sensing paths on identifying the damage in the composite panel is investigated. The results demonstrate that the diagnostic algorithm, being computationally efficient and amenable to automated processing, can be used to identify damage in highly complex structures.

1. Introduction

Interrogation algorithms using ultrasonic guided waves have been a topic of considerable interest for nondestructively inspecting structural integrity [1–7]. For guided wave-based structural health monitoring (GW-SHM) algorithms, to identify the presence of damage and characterize it in terms of location and severity, damage signatures are extracted and interpreted from the acquired wave signals. Several guided wave features, including the time-of-flight (ToF), propagation velocity, and wavelet coefficients have been elaborated in terms of sensitivity to different types of damage. Among them, ToF-based algorithms have received a great deal of attention, being acknowledged as effective candidates for damage identification in many cases [8–12].

It is well documented that Lamb waves, among the most commonly used ultrasonic guided waves for SHM purposes, may have multiple modes, excited at a certain central frequency, accompanied by possible dispersion. Although conscientious efforts have been made to improve the resolution of ToF-based algorithms, including the classical thresholding procedure and the envelope algorithm [13–17], it is still fairly problematic to identify particular wave modes of each reflected/transmitted wave component and decide precisely the corresponding ToF. This drawback is particularly amplified and becomes a big challenge for damage identification in highly complex structures, given that hidden damage signatures can be easily overwhelmed by the complex propagation characteristics of Lamb waves caused by geometric complexities. On the other hand, an alternative algorithm has been developed, namely probabilistic inspection strategy based on correlation analysis [18–21], which does not rely on the extraction of detailed signatures about each wave component in the acquired wave signals. Such a diagnostic algorithm focuses on integrated changes in signals due to the presence of damage, and it is based on correlation coefficients of Lamb wave signals from selected sensing paths in the present (with damage) and the reference (without damage) states.

The objective of this study is to evaluate the capability of this diagnostic algorithm for identifying damage in a composite panel of five stiffeners, where conventional ToF-based algorithms may not be applicable, using the estimated probability of the presence of damage in the monitoring area enclosed by an active sensor network. The effects of the networks of sensing paths and the shapes of the affected zone of individual sensing paths on locating the damage are also discussed.

* Corresponding author. Address: Laboratory of Smart Materials and Structures (LSMS), Centre for Advanced Materials Technology (CAMT), School of Aerospace, Mechanical and Mechatronic Engineering, The University of Sydney, NSW 2006, Australia. Tel.: +61 2 9351 4798; fax: +61 2 9351 3760.
E-mail address: l.ye@usyd.edu.au (L. Ye).

0266-3538/$ - see front matter © 2008 Elsevier Ltd. All rights reserved.
doi:10.1016/j.compscitech.2008.11.005

这里Ri和β都比常规大1

2. Probability of the presence of damage

For estimating the probability of the presence of damage in the monitoring area, the correlation of Lamb wave signals in two different states, viz. the present and the reference states, plays an essential role in this study. The correlation of the two signals offers a clue as to how well one signal can be approximated by the other [22]. The correlation coefficient of two variables, $x = \{x_1, x_2, ..., x_n\}$ and $y = \{y_1, y_2, ..., y_n\}$, is defined in terms of their covariance, $cov(x,y)$, and standard deviations, σ_x and σ_y.

$$\rho_{x,y} = \frac{cov(x,y)}{\sigma_x \sigma_y} \tag{1}$$

For GW-SHM algorithms, it is well accepted that the wave signals from a selected sensing path contain information about structural integrity. In this study, the presence of damage is assumed to be the exclusive reason for the changes in Lamb wave signals between the reference and present states. The changes induced by other factors in practical application, e.g. the environmental noise in other frequency range, could be filtered out by employing advanced signal processing methods. The degree of signal change for a particular sensing path before and after damage is introduced will clearly be increased if the sensing path is close to the damage and conversely will be decreased if the sensing path is distant from the damage. It is evident that the correlation coefficients for seriously damage-impaired sensing paths are lower than those for slightly damage-impaired sensing paths. As a result, a hotspot in the monitoring area can be considered as the common area which is near most of the seriously damage-impaired sensing paths with low correlation coefficients. On the basis of this principle, the complexity of structural geometry or boundary condition would not affect the capability of the proposed algorithm for damage identification, as these influences are implicitly included in both the reference and present signals.

The monitoring area is meshed into uniformly distributed grids and the probability of the presence of damage at each grid is estimated. For any grid, the correlation coefficient from each sensing path presents an estimation of the probability of the presence of damage at this position. Different weights, which are measured by the distances from the grid to the selected sensing paths, are included in the final decision fusion. The area consisting of the grids with probability values for the presence of damage above a specified threshold is defined as the damaged area. In particular, the grid with the highest probability value for the presence of damage indicates the centre of the identified damage. Assuming there are N sensing paths in total, the estimation at position (x,y) can be written as [20]

$$P(x,y) = \sum_{k=1}^{N} p_k(x,y) = \sum_{k=1}^{N} A_k \left[\frac{-1}{\beta - 1} \cdot R(x,y,x_{ak},y_{ak},x_{sk},y_{sk}) + \frac{\beta}{\beta - 1} \right] \tag{2}$$

where

$$R(x,y,x_{ak},y_{ak},x_{sk},y_{sk}) = \begin{cases} R_c(x,y,x_{ak},y_{ak},x_{sk},y_{sk}), & R_c(x,y,x_{ak},y_{ak},x_{sk},y_{sk}) < \beta \\ \beta, & R_c(x,y,x_{ak},y_{ak},x_{sk},y_{sk}) \geq \beta \end{cases} \tag{3}$$

and

$$R_c(x,y,x_{ak},y_{ak},x_{sk},y_{sk}) = \frac{\sqrt{(x-x_{ak})^2 + (y-y_{ak})^2} + \sqrt{(x-x_{sk})^2 + (y-y_{sk})^2}}{\sqrt{(x_{ak}-x_{sk})^2 + (y_{ak}-y_{sk})^2}} \tag{4}$$

is the ratio of the sum of the distances from the grid (x,y) to the actuator (x_a,y_a) and to the sensor (x_s,y_s) to the distance between the actuator and sensor. $p_k(x,y)$ is the estimation of probability of the presence of damage from the kth sensing path, and $A_k = 1 - \rho_k$ is the input feature of the kth sensing path, ρ_k is the correlation coefficient between the present signals and the reference signals from the kth sensing path. β is a scaling parameter which controls the size of the affected zone of sensing paths.

The affected zone can be elaborated by an ellipse encircling an actuator-sensor pair (sensing path), if it is assumed that the velocity of the wave signal is constant, illustrated in Fig. 1 [20]. The shape of the ellipse can be expressed by its eccentricity, denoted by ε. For an ellipse with semi-major axis, a, semi-minor axis, b, and the distance from the centre to either focus, c, the eccentricity is $\varepsilon = \sqrt{1 - b^2/a^2} = c/a$. The greater the eccentricity, the greater the ratio of c to a, and thus the more elongated the ellipse. In this study, the scaling parameter, β, can be designated as the reciprocal of eccentricity, ε, i.e. $\varepsilon = 1/\beta$. Therefore, the lower the scaling parameter, the more elongated is the affected zone [20].

3. Specimen and experimental set-up

β为离心率的倒数
β越小，椭圆越长

A composite panel of the dimensions $900 \times 560 \times 1.6\ mm^3$ as shown schematically in Fig. 2 was used in this study. The panel has five co-cured composite stiffeners (height: 26 mm, length: 670 mm, thickness: 2 mm) and a circular hole (diameter: 50 mm). The lay-up contains 12 plies with a configuration of $[0/\pm 45_2/90/0_2]_s$. Artificial damage was introduced in the form of a through-thickness hole with a diameter of 11.9 mm in a half section of the panel (Fig. 2). The active sensor network was configured by 18 piezoelectric ceramic discs (PZT PI® PIC151, PRYY-0929) with a diameter of 6.9 mm and 0.5 mm in thickness. They were surface-

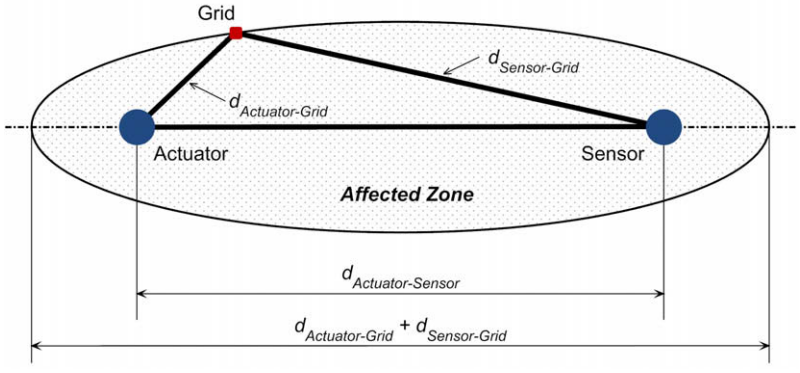

Fig. 1. Diagram of affected zone of individual sensing paths (ellipse distribution).

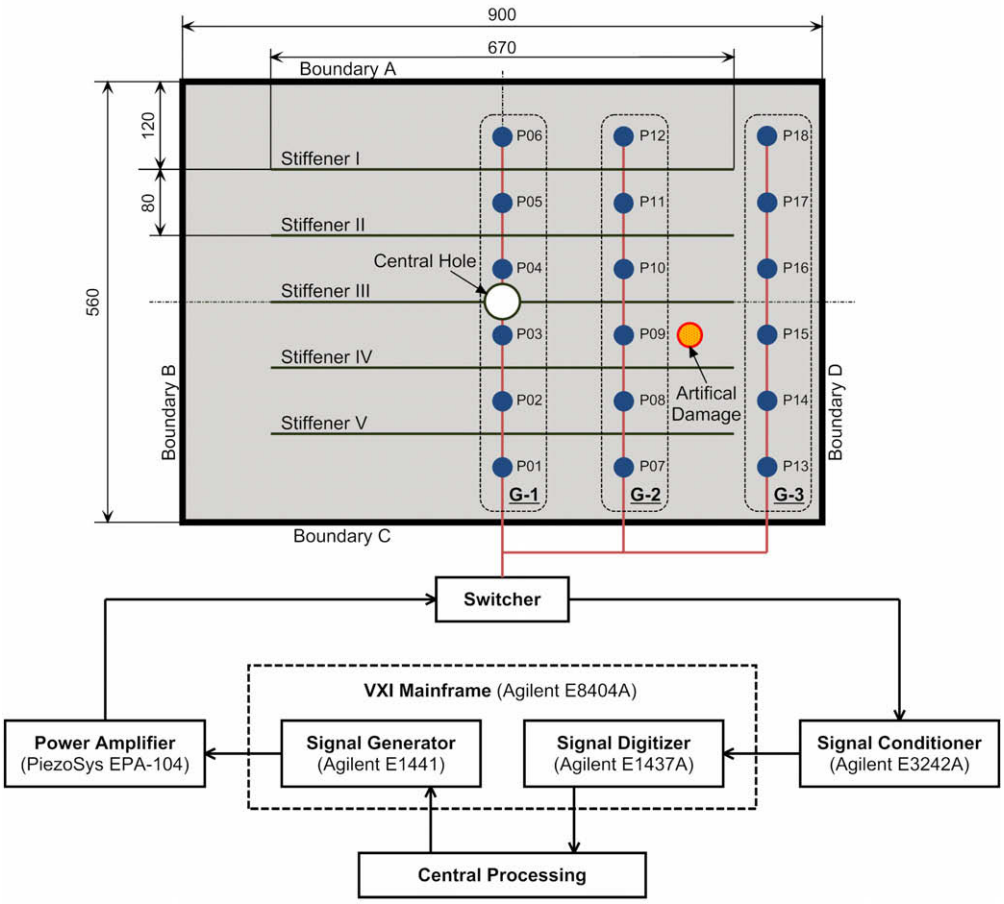

Fig. 2. Geometry of composite panel and the experimental set-up.

mounted in the half section of the panel (Fig. 2) in three parallel lines using a silver-filled epoxy adhesive (RiteLok® SL65), denoted by G-1, G-2 and G-3, respectively. A photograph of the composite panel with the active sensor network installed is presented in Fig. 3. The monitoring area enclosed by the PZTs has the dimensions of $400 \times 385\ mm^2$. A coordinate system (Fig. 4) was employed with the plane of the monitoring area spanned by the horizontal, x, and vertical, y, axes, where the origin of coordinate was set to be the centre of P06. The coordinate of the centre of actual damage was ($x = 225$ mm, $y = 240$ mm).

The experimental set-up is shown schematically in Fig. 2. In this study, a 5-cycle sinusoidal toneburst (60 V peak-to-peak) enclosed in a Hanning window at a central frequency of 300 kHz was gener-

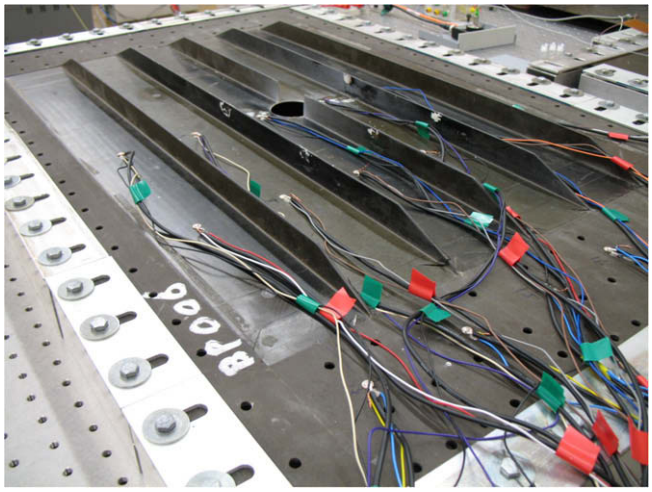

Fig. 3. The composite panel with the active sensor network installed.

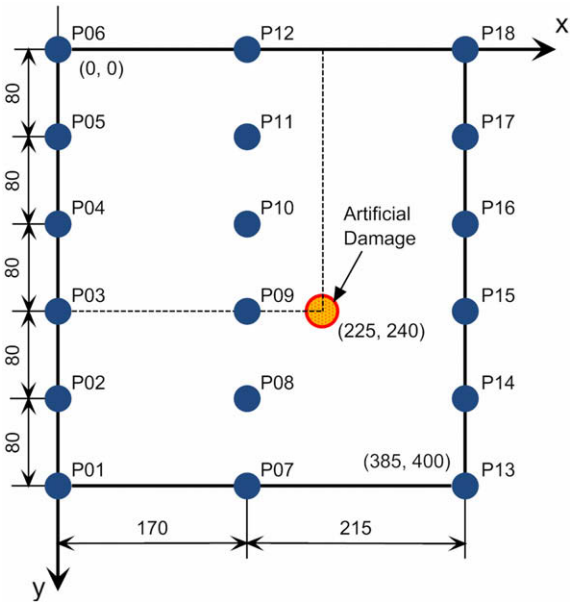

Fig. 4. The coordinate system of the monitoring area.

ated as the input signal for the active sensor network. The sampling rate was set at 20.48 MHz. Activation and acquisition of Lamb wave signals were fulfilled using an active signal generation and data acquisition system developed on the VXI platform, illustrated in Fig. 2, where the direction of the flow of data is indicated by arrows. While one of the PZT elements in the active sensor network acts as the actuator to generate Lamb waves, the others function as sensors to capture Lamb wave signals propagating in the panel. Although the damage may not be discemible from one particular sensing path, it may be apparent from others. Thus many sensing paths are employed to interrogate the presence of damage. The current active sensor network (18 PZTs in three parallel lines) provides 306 cross-sensing paths in total. However, only the sensing paths that pass through the monitoring area are of interest for interrogation of the probability of the presence of damage, where the sensing paths establish cross-interrogation covering the monitoring area, illustrated in Fig. 5. It is noted that interrogation of G-1/G-3 emphasizes global information (the entire monitoring area); whereas interrogation of G-1/G-2 and G-2/G-3 emphasizes local information (left or right parts of the monitoring area).

4. Interrogation of Lamb wave signals

Lamb wave signals from the selected sensing paths (Fig. 5) were captured experimentally in both the reference and present states (before and after the artificial damage was introduced). The signals from two different sensing paths, P15-P09 and P14-P08, are displayed in Fig. 6. The solid lines represent the signals in the reference state, while the dashed lines represent the signals in the present state. For each captured wave signal, after marginal electromagnetic interference, the first observed wave component is associated with the transmitted fundamental symmetric Lamb mode, S_0, due to its fastest propagation velocity, although it may also include interference if the sensing path crosses any stiffeners. The signals were normalized using the peak amplitude of the transmitted S_0 mode in the reference state. A noticeable decrease in the amplitude of the transmitted S_0 mode between the two states was observed for the signals from sensing path P15-P09, displayed in Fig. 6a. This decrease was attributed to the fact that this sensing path passed directly through the damage, and was seriously impaired by the damage. In contrast, no such a phenomenon was evident for the signals from sensing path P14-P08, displayed in Fig. 6b, for the reason that this sensing path was located relatively distant from the damage, and was only slightly impaired by the damage.

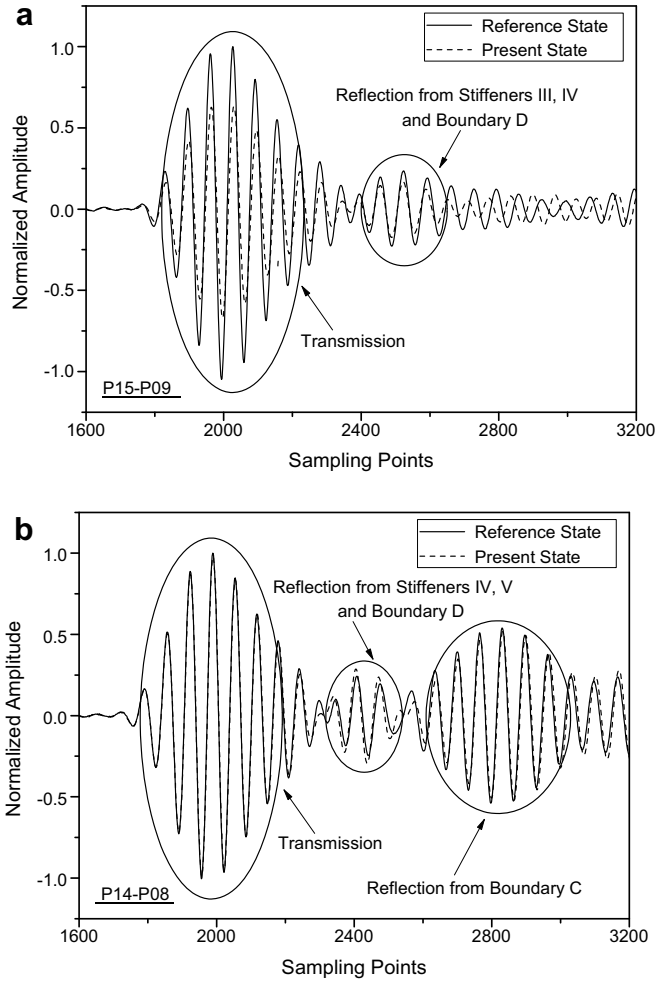

Fig. 6. Captured Lamb wave signals from different sensing paths: (a) P15-P09; (b) P14-P08.

On the basis of the propagation distances, after the transmitted S_0 mode, the next observed wave component in Fig. 6 was the combination of the reflected S_0 mode from the closest stiffeners (III and IV for path P15-P09, IV and V for path P14-P08) and the reflected S_0

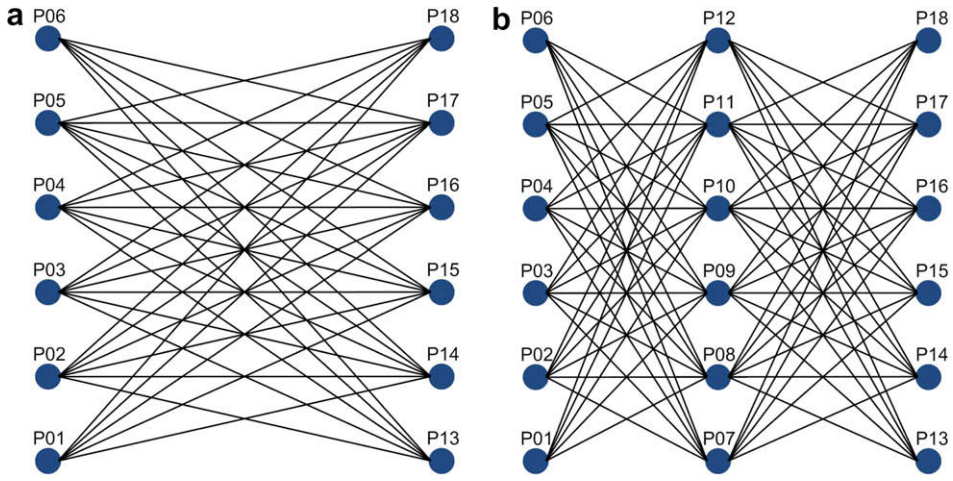

Fig. 5. Different networks of sensing paths: (a) global interrogation (G-1/G-3); (b) local interrogations (G-1/G-2, G-2/G-3).

mode from boundary D. Additionally, since sensing path P14-P08 was close to boundary *C*, an extra reflected S_0 mode from boundary *C* is observed in Fig. 6b, but no such a component is observed in Fig. 6a. For such a complex structure, it is appreciated that the damage-induced wave component would easily be overwhelmed by reflection from the stiffeners and boundaries. Differentiation of these overlapping components is difficult, not to mention precise extraction of the associated ToF. Therefore, it can be concluded that conventional ToF-based algorithms [13,15] are problematic for such a complex structure, which is where the new diagnostic algorithm makes an important contribution.

All the sampling points between the end of the electromagnetic interference and the end of the transmitted S_0 mode were employed to calculate the correlation coefficients for the selected sensing paths. Fig. 7 plots the correlation coefficients in radar charts for the selected sensing paths in Fig. 5. Each hexagon pre-

可读性较差

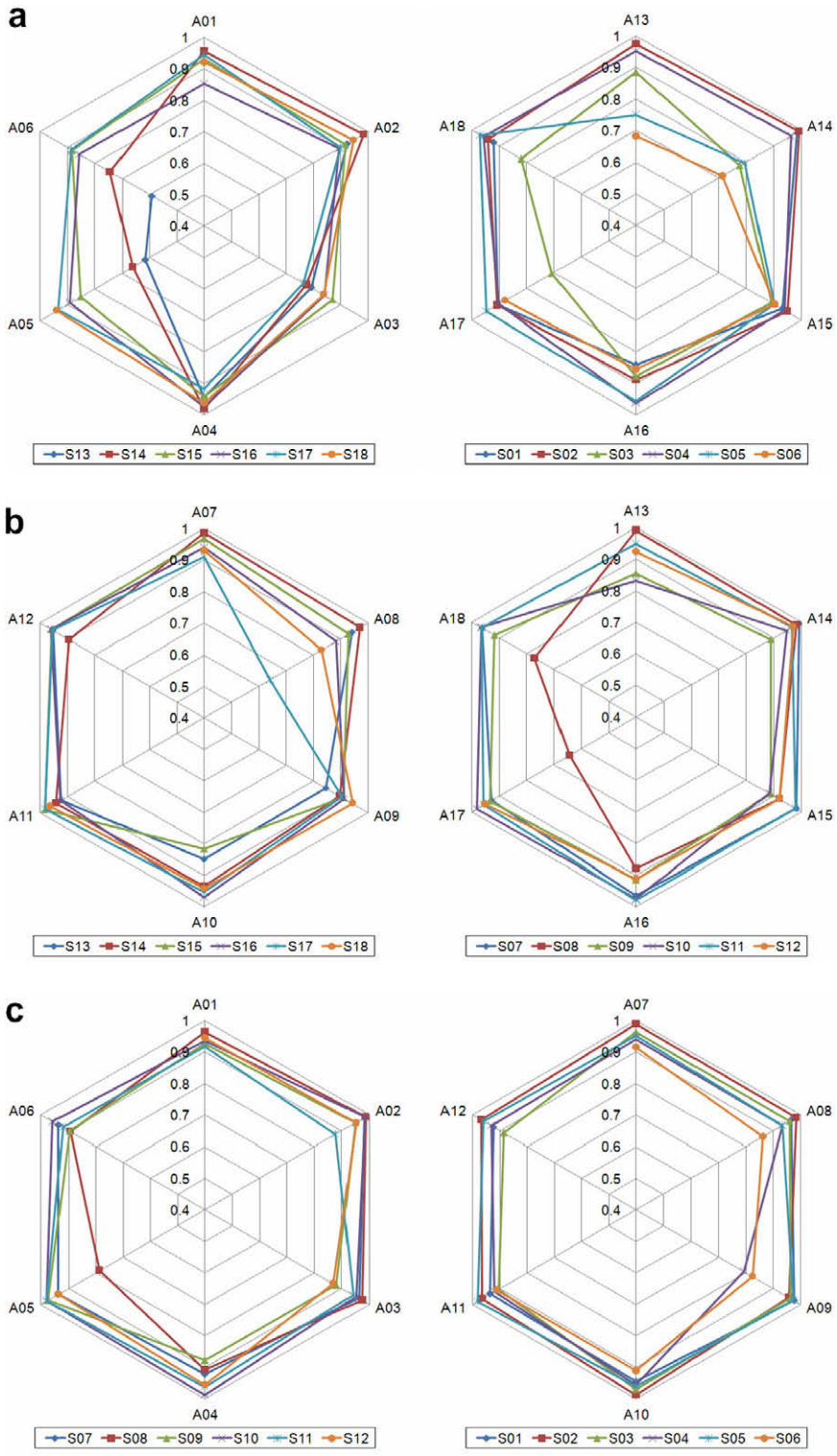

Fig. 7. Correlation coefficients for different sensing paths: (a) G-1/G-3; (b) G-2/G-3; (c) G-1/G-2.

sents the correlation coefficients for a group of sensing paths with the same sensor but six different actuators. The smaller the distance from a certain vertex to the origin of a hexagon, the lower the correlation coefficient is, implying more drastic changes in signals for this sensing path due to the presence of damage. The correlation coefficients for sensing paths P_i–P_j and P_j–P_i were not identical, because of interference from the stiffeners, central hole and boundaries, besides the transmitted S_0 mode. The results from the global interrogation of G-1/G-3 are illustrated in Fig. 7a. Several sensing paths have correlation coefficients lower than 0.80, among which P06-P13 and P13-P06 have the lowest values, demonstrating that the signals from these two sensing paths changed substantially due to the presence of damage. The results confirm that damage exists in the monitoring area; otherwise all the hexagons would maintain the same regular shape (i.e. $\rho_{x,y}$ is close to 1.00 for all vortexes). A similar phenomenon was also observed for the results of the local interrogation of G-2/G-3, illustrated in Fig. 7b. Several sensing paths have correlation coefficients lower than 0.80, among which P08-P17 and P17-P08 have the lowest values. However, as observed in the results of the local interrogation of G-1/G-2, illustrated in Fig. 7c, most of sensing paths had correlation coefficients approximately equal to 1.00, although with some exceptions because of other interference, indicating that the signals were not strongly associated with the presence of damage. Based on the correlation coefficients in Fig. 7, it can be concluded that the hotspot representing the location of damage should be in the area between G-2 and G-3.

划分区域：7c图都大约为1，说明该区域与损伤关系不大

5. Damage identification

5.1. Different networks of sensing paths

In estimating the probability of the presence of damage in the monitoring area, different networks of sensing paths were established and their performance was investigated. The simple network of sensing paths was based on global interrogation which included 68 paths, displayed in Fig. 5a. The intermediate network of sensing paths combined two local interrogations which included 136 paths,

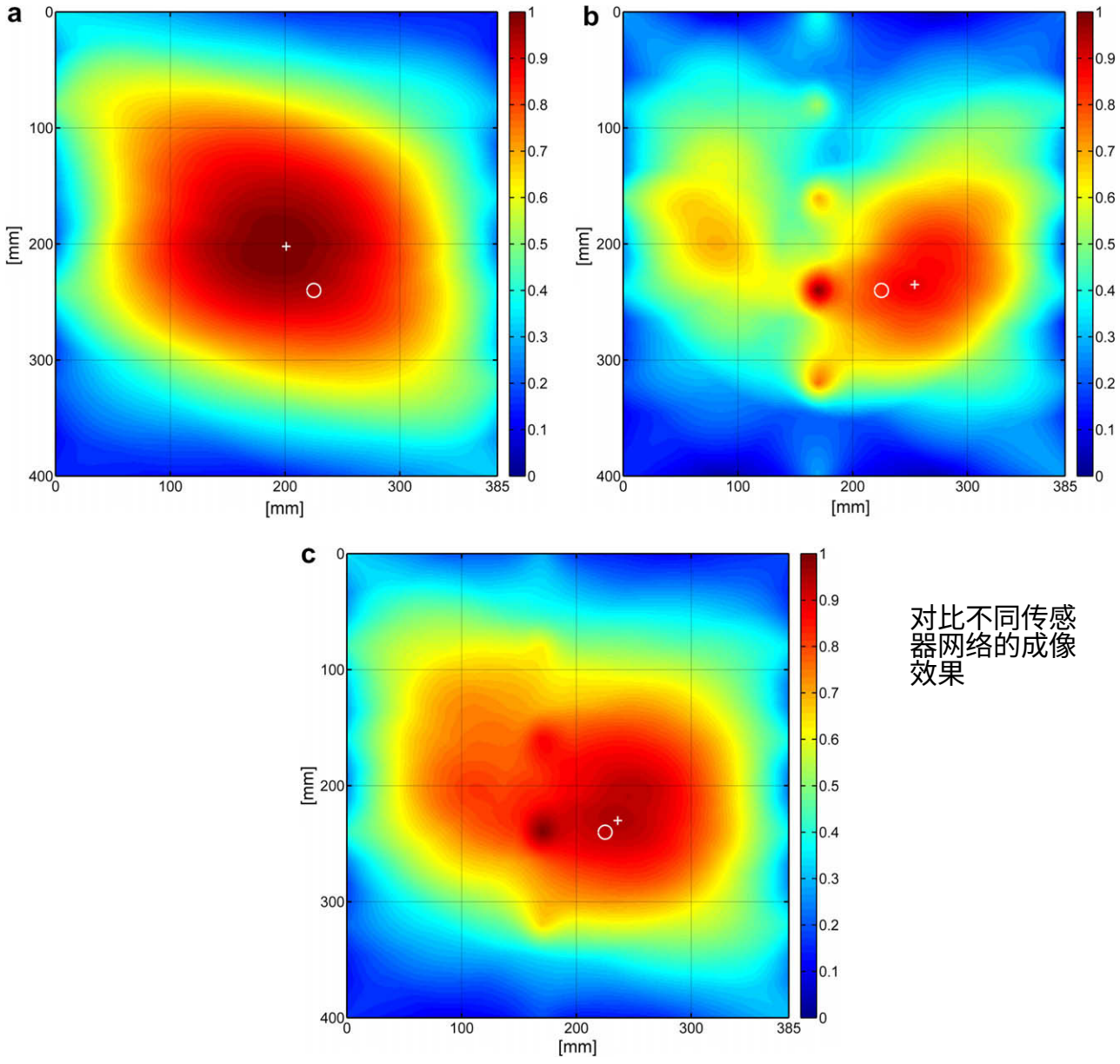

对比不同传感器网络的成像效果

Fig. 8. The probability of the presence of damage estimated using different networks of sensing paths ($\beta = 1.15$): (a) simple; (b) intermediate; (c) advanced.

displayed in Fig. 5b. The advanced network of sensing paths involved both global and local interrogations simultaneously which included 204 paths. In this study, 400 × 385 uniformly distributed grids were meshed in the monitoring area (400 × 385 mm^2) to define the probability of the presence of damage.

In the algorithm, the scaling parameter, β, was firstly set at 1.15. Fig. 8 illustrates the probability of the presence of damage estimated using the three networks of sensing paths. The contour graphs have the dimensions of 400 × 385 mm^2, being the same as the monitoring area in the composite panel. The small solid circle indicates the location of actual damage (diameter: 11.9 mm). The area consisting of the grids with relatively high probability values for the presence of damage was determined by the probability of the presence of damage estimated using the simple network of sensing paths, illustrated in Fig. 8a, which demonstrates that damage must exist in the monitoring area. In addition, based on the probability of the presence of damage estimated using the intermediate network of sensing paths, illustrated in Fig. 8b, the damage was further identified in the right part of the monitoring area. Finally, the damage was identified successfully using the probability of the presence of damage estimated using the advanced network of sensing paths, illustrated in Fig. 8c. The grid with the highest probability value for the presence of damage, indicated by the small cross, was considered as the centre of identified damage. It is observed that when using the intermediate and advanced networks of sensing paths with β = 1.15, the grid with the highest probability value for the presence of damage falls at the centre of P09. This is attributed to the fact that P09 is very close to the actual damage and it provides a large number of dominant damage-impaired sensing paths, which leads to the extremely high probability value for the presence of damage at this location. As a result, these points coincident with the locations of the sensors allocated within the monitoring area should be excluded because they are the pseudo-presence of damage. Table 1 compares the results using the three networks of sensing paths in terms of the relative distance between the centre of identified damage and that of the actual damage. Identification using the advanced network of sensing paths agreed well with the actual damage location, whereas identification using the simple and intermediate networks of sensing paths was insufficiently accurate. The results demonstrate that the resolution of this diagnostic algorithm is highly dependent on the network of sensing paths.

For any network of sensing paths, theoretically, if none of the sensing paths is damage-impaired, such a network cannot pinpoint the damage. Therefore, to focus on the hotspot representing the damage location and eliminate misleading information, the network of sensing paths was further improved. An optimized network of sensing paths, including 136 paths, was obtained by removing the local interrogation of G-1/G-2 from the advanced network of sensing paths. Fig. 9 illustrates the probability of the presence of damage estimated using such an optimized network of sensing paths. Consequently, the area consisting of grids with probability values for the presence of damage above the specified thresholds (set at 90%, 95%, 97% and 99%) are plotted in Fig. 10. The identified area (when threshold = 90%, 95% and 97%) covers the actual damage or closes to it (when threshold = 99%). The results lead to the conclusion that the diagnostic algorithm is capable of pinpointing damage in such a complex composite structure if appropriate sensing paths are included in the interrogation.

Table 1
Effect of different networks of sensing paths on the location of identified damage (β = 1.15).

Network	Coordinates (mm)	Relative distance (mm)
Simple	(201,202)	44.94
Intermediate	(254,235)	29.43
Advanced	(236,230)	14.87

5.2. Different shapes of affected zone

In addition to the network of sensing paths, the estimation of the probability of the presence of damage is also affected by the shape of the affected zone of individual sensing paths. Considering the rather dense sensing paths in the current configuration, the scaling parameter, β, was set at 1.05, 1.10, 1.20 and 1.25, to investigate its effect on identifying the damage in the composite panel. The probabilities of the presence of damage estimated using optimized network of sensing paths with different scaling parameters are illustrated in Fig. 11. The areas consisting of grids with proba-

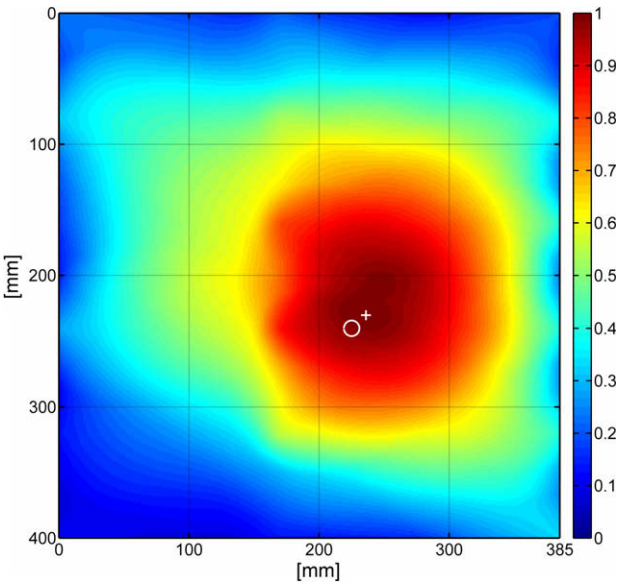

Fig. 9. The probability of the presence of damage estimated using the optimized network of sensing paths (β = 1.15).

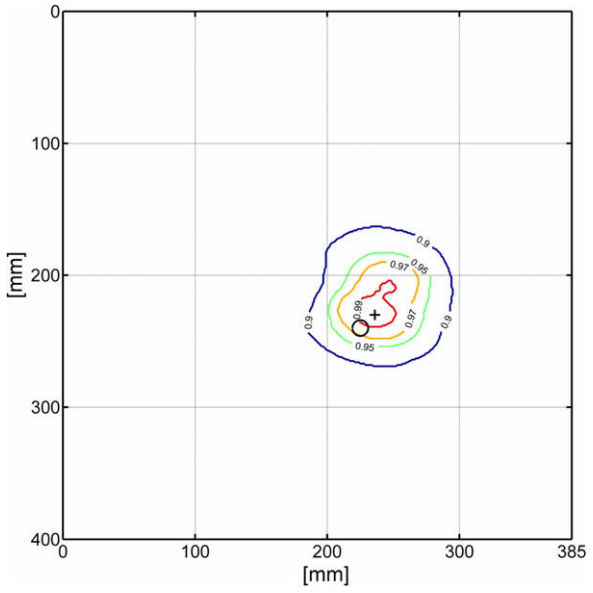

Fig. 10. Areas with probability values for the presence of damage above the thresholds using the optimized network of sensing paths (β = 1.15).

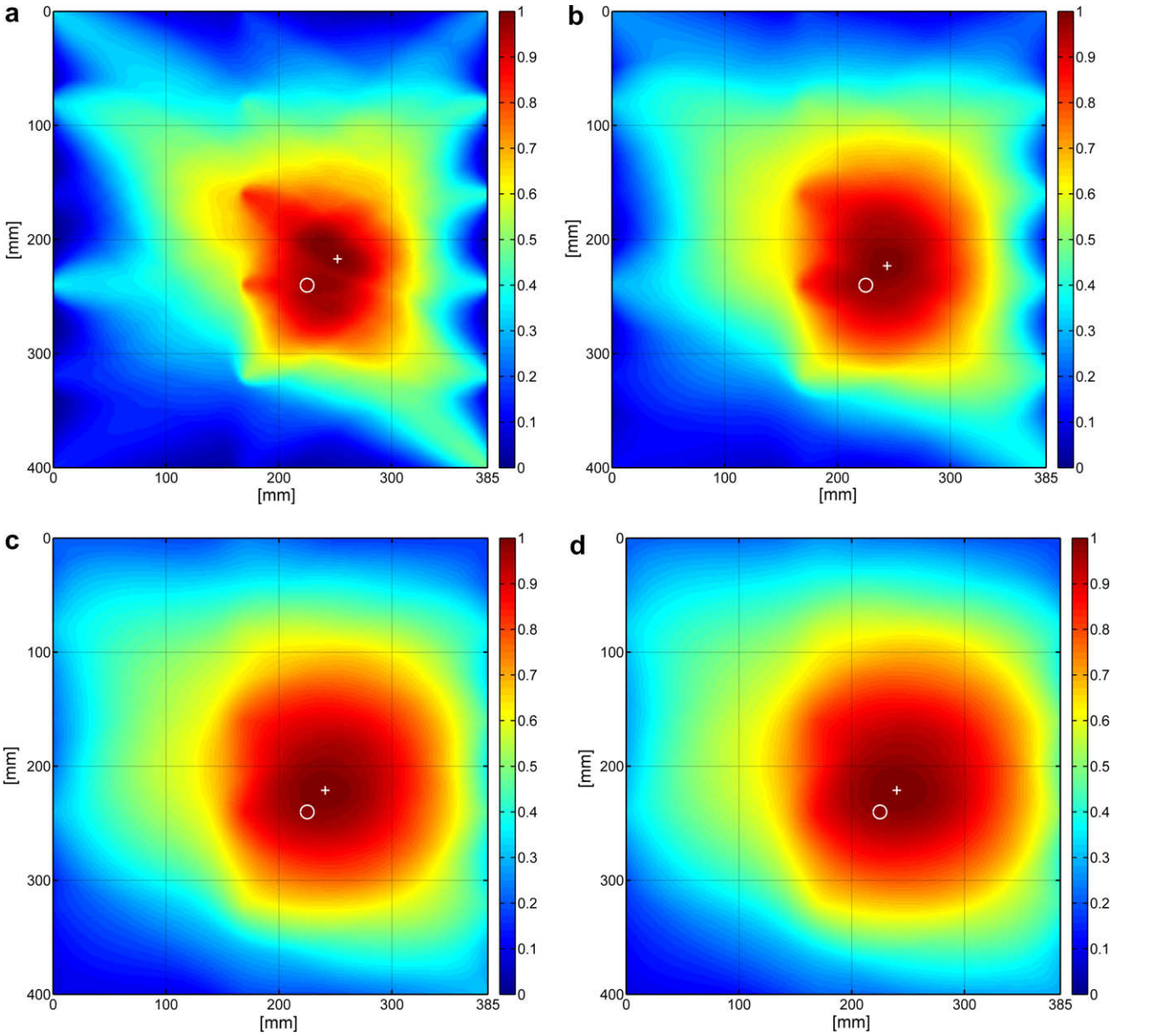

Fig. 11. The probability of the presence of damage estimated using the optimized network of sensing paths with different scaling parameters: (a) $\beta = 1.05$; (b) $\beta = 1.10$; (c) $\beta = 1.20$ and (d) $\beta = 1.25$.

bility values for the presence of damage above the thresholds (90%, 95%, 97% and 99%) are plotted in Fig. 12. It is observed that the identified areas are reduced when $\beta = 1.05$ or 1.10 in comparison with those in Fig. 10 (when $\beta = 1.15$), for the reason that a small scaling parameter reduces the affected zone, making the diagnostic algorithm sensitive. Conversely, the identified areas are enlarged when $\beta = 1.20$ or 1.25, for the reason that a large scaling parameter enlarges the affected zone, making the diagnostic algorithm conservative. The locations of the damage identified using the different scaling parameters are summarized in Table 2. The best result identified was obtained using the optimized network of sensing paths when $\beta = 1.15$.

β取值的探讨

6. Conclusions

A guided wave-based algorithm for damage identification by estimating the probability of the presence of damage was evaluated using an active sensor network in structures with complex geometry. Such a diagnostic algorithm does not rely on the extraction of detailed information of each wave component, which is problematic for complex structures. The algorithm was validated experimentally by locating artificial damage in the form of a through-thickness hole (diameter: 11.9 mm) in a composite panel of five stiffeners, where an active sensor network of 18 PZT elements was utilized to provide wave signals for interrogation before and after the damage was introduced. The area consisting of grids with probability values for the presence of damage above the thresholds clearly covers or closes to the actual damage in the composite panel. The employment of more damage-impaired sensing paths can considerably improve the resolution of the estimation, whereas the shape of the area consisting of grids with probability values for the presence of damage above the threshold changes only a little when the scaling parameter is selected in an appropriate range. The results presented in this study demonstrate that the estimated probability of the presence of damage in the monitoring area can be used to characterize damage in highly complex structures.

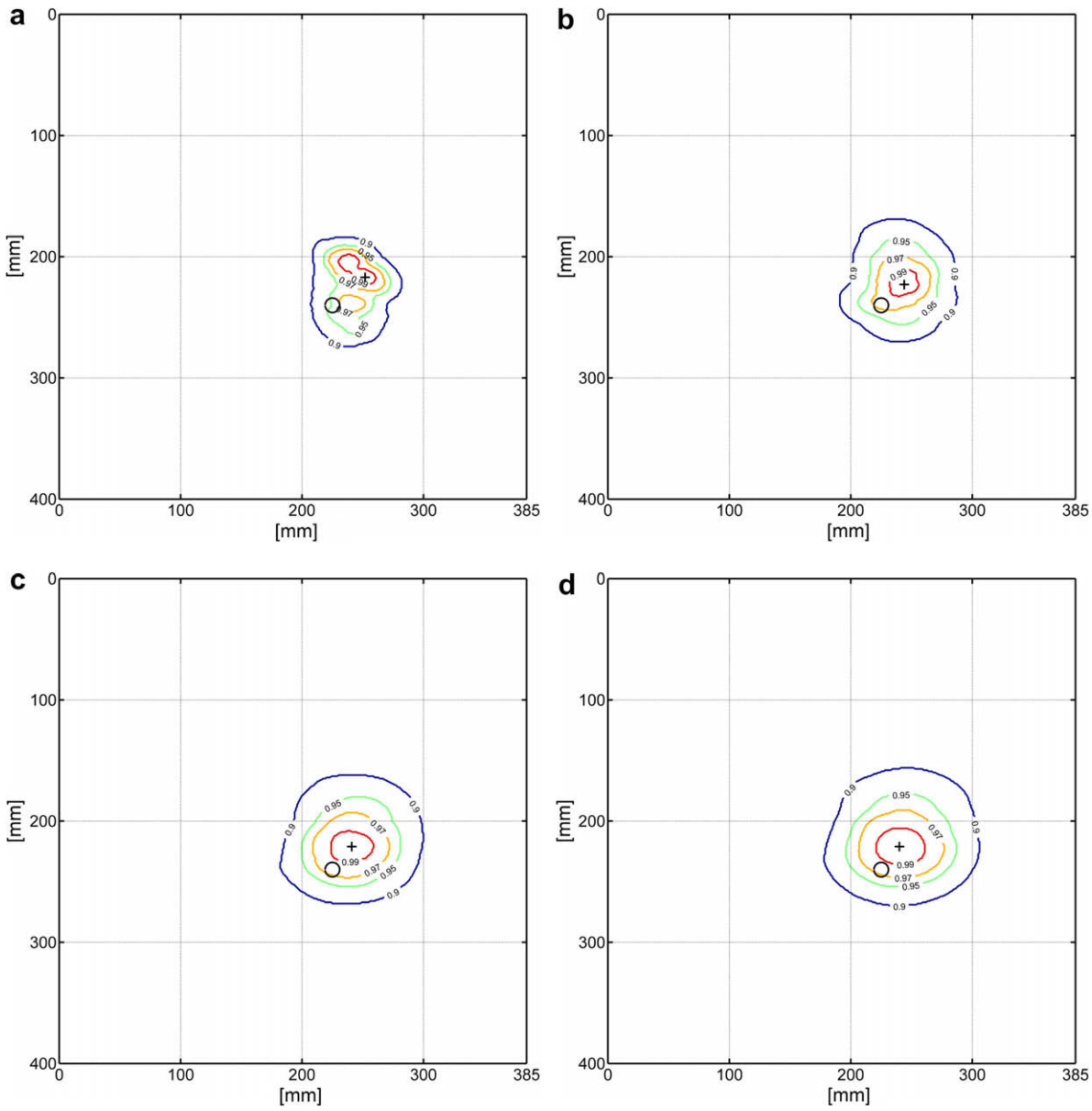

Fig. 12. Areas with probability values for the presence of damage above the thresholds using the optimized network of sensing paths with different scaling parameters: (a) $\beta = 1.05$; (b) $\beta = 1.10$; (c) $\beta = 1.20$ and (d) $\beta = 1.25$.

Table 2
Effect of different scaling parameters on the location of identified damage (optimized network).

Scaling parameter	Coordinates (mm)	Relative distance (mm)
1.05	(252,217)	35.47
1.10	(244,223)	25.50
1.15	(236,230)	14.87
1.20	(241,221)	24.84
1.25	(240,221)	24.21

Acknowledgements

D. Wang is supported by a Faculty Scholarship and a Scholarship in Structural Health Monitoring from The University of Sydney, Australia. L. Ye is grateful for the research support of a Discovery Project (DP) from the Australian Research Council. Z. Su is grateful to the Research Grants Council of Hong Kong for General Research Fund (GRF) 527008. The authors are grateful for the support of CRC-ACS (Cooperative Research Centre for Advanced Composite Structures Ltd.) in providing the composite panel.

References

[1] Rose JL, Avioli MJ, Mudge P, Sanderson R. Guided wave inspection potential of defects in rail. NDT&E Int 2004;37(2):153–61.
[2] Ye L, Su Z, Yang C, He Z, Wang X. Hierarchical development of training database for artificial neural network-based damage identification. Compos Struct 2006;76(3):224–33.
[3] Lanza Discalea F, Matt H, Bartoli I, Coccia S, Park G, Farrar C. Health monitoring of UAV wing skin-to-spar joints using guided waves and macro fiber composite transducers. J Intell Mater Syst Struct 2007;18(4):373–88.
[4] Michaels JE, Michaels TE. Guided wave signal processing and image fusion for in situ damage localization in plates. Wave Motion 2007;44(6):482–92.
[5] Raghavan A, Cesnik CES. Guided-wave signal processing using chirplet matching pursuits and mode correlation for structural health monitoring. Smart Mater Struct 2007;16(2):355–66.
[6] Staszewski WJ, Lee BC, Traynor R. Fatigue crack detection in metallic structures with Lamb waves and 3D laser vibrometry. Measure Sci Technol 2007;18(3):727–39.

[7] Diamanti K, Soutis C, Hodgkinson JM. Piezoelectric transducer arrangement for the inspection of large composite structures. Compos Part A: Appl Sci Manuf 2007;38(4):1121–30.
[8] Su Z, Ye L. Lamb wave-based quantitative identification of delamination in CF/EP composite structures using artificial neural algorithm. Compos Struct 2004;66(1–4):627–37.
[9] Meo M, Zumpano G, Piggott M, Marengo G. Impact identification on a sandwich plate from wave propagation responses. Compos Struct 2005;71(3–4):302–6.
[10] Tua PS, Quek ST, Wang Q. Detection of cracks in cylindrical pipes and plates using piezo-actuated Lamb waves. Smart Mater Struct 2005;14(6):1325–42.
[11] Su Z, Wang X, Chen Z, Ye L, Wang D. A built-in active sensor network for health monitoring of composite structures. Smart Mater Struct 2006;15(6):1939–49.
[12] Quek ST, Tua PS, Jin J. Comparison of plain piezoceramics and inter-digital transducer for crack detection in plates. J Intell Mater Syst Struct 2007;18(9):949–61.
[13] Su Z, Ye L. Fundamental Lamb mode-based delamination detection for CF/EP composite laminates using distributed piezoelectrics. Struct Health Monit 2004;3(1):43–68.
[14] Li F, Su Z, Ye L, Meng G. A correlation filtering-based matching pursuit (CF-MP) for damage identification using Lamb waves. Smart Mater Struct 2006;15(6):1585.
[15] Lu Y, Ye L, Su Z. Crack identification in aluminium plates using Lamb wave signals of a PZT sensor network. Smart Mater Struct 2006;15(3):839–49.
[16] Lee BC, Staszewski WJ. Lamb wave propagation modelling for damage detection: II. Damage monitoring strategy. Smart Mater Struct 2007;16(2):260–74.
[17] Wang D, Ye L, Su Z, Lu Y. Identification of dual damage in woven fabric composite beams using low frequency A_0 Lamb mode. In: Fourteenth international conference on composite structures (ICCS14), Melbourne, Victoria, Australia; 2007.
[18] Gao H, Shi Y, Rose JL. Guided wave tomography on an aircraft wing with leave in place sensors. In: Review of progress in quantitative nonstructive evaluation. Golden (CO, USA): AIP; 2005.
[19] Hay TR, Royer RL, Gao H, Zhao X, Rose JL. A comparison of embedded sensor Lamb wave ultrasonic tomography approaches for material loss detection. Smart Mater Struct 2006;15(4):946–51.
[20] Zhao X, Gao H, Zhang G, Ayhan B, Yan F, Kwan C, et al. Active health monitoring of an aircraft wing with embedded piezoelectric sensor/actuator network: I. Defect detection, localization and growth monitoring. Smart Mater Struct 2007;16(4):1208–17.
[21] Wang D, Ye L, Lu Y, Li F. Diagnostics of damage presence using tomographically constructed probability distribution based on Lamb wave signals. In: Fourth European workshop on structural health monitoring (EWSHM-4), Kraków, Poland; 2008.
[22] Cohen J, Cohen P, West SG, Aiken LS. Applied multiple regression/correlation analysis for the behavioral sciences. London: Lawrence Erlbaum Associates; 2003.